32nd URSI GASS, Montreal, 19–26 August 2017

Constraining Ionospheric Models with Radio Interferometric Self-Calibration Data

Stefan J. Wijnholds
ASTRON, Oude Hoogeveensedijk 4, 7991 PD, Dwingeloo, The Netherlands, wijnholds@astron.nl

Abstract

Radio interferometers can measure the differential total electron content (TEC) between pairs of lines-of-sight through the ionosphere above the interferometric array very accurately. Such data potentially forms a nice complement to the absolute TEC measurements from GPS receiver networks that usually provide data with lower spatial sampling density and lower accuracy. This paper presents an overview of currently used ionospheric calibration schemes in radio astronomy. For each method, I describe how the data takes care of the 3-D structure of the ionosphere, quantify the accuracy of the differential TEC measurements and discuss the spatial sampling density.

1 Introduction

The raw data used in many ionospheric studies are provided by networks of GPS receivers [1, 2]. These data typically provide reasonably accurate ($\sim$ 10 to $\sim$ 100 mTECU, 1 TECU $= 10^{16}$ m^{-2}) measurements of the absolute total electron content (TEC) with a spatial separation of $\sim$ 100 km. In contrast, radio interferometric self-calibration data typically provide highly accurate ($\sim$ 1 mTECU) measurements of the differential TEC between pairs of lines-of-sight through the ionosphere. The distance between the lines-of-sight constituting a pair may range from several tens of meters to several hundreds of kilometers, depending on the distribution of the receiving elements of the interferometer array.

In this paper, I give an overview of currently used ionospheric calibration schemes in radio astronomy and discuss how each method accounts for the 3-D structure of the ionosphere. I also quantify the accuracy of the differential TEC measurements obtained and the spatial sampling density based on available source statistics.

Different approaches to ionospheric calibration have been developed for different radio astronomical instruments. For the purpose of the current discussion, these approaches can be divided into two categories: schemes that have been developed for interferometric arrays whose extend is smaller than the typical diffractive scale of the ionosphere and methods that have been developed for instruments with baselines (much) longer than the typical diffractive scale of the ionosphere. These two categories are discussed in the next two sections. Before concluding the paper, I discuss the merits of using a single ionospheric model for the entire array or using an individual ionospheric model for each receiving element in the array in Sec. 4.

2 Measurements with small arrays

The TEC of the ionosphere along a given line-of-sight causes the radio signal propagating along that line-of-sight with frequency ν to experience an additional phase delay (measured in radians) of [3]

$$\phi = -8.45 \left(\frac{\text{TEC}}{1\ \text{TECU}} \right) \left(\frac{\nu}{1\ \text{GHz}} \right)^{-1}. \qquad (1)$$

For each pair of receiving elements, a radio interferometric array measures the phase difference between the line-of-sight from the first receiving element of the interferometer to a source and the line-of-sight from the second receiving element to the same source. To see what this implies for the accuracy to which radio interferometers can measure the differential TEC between two lines-of-sight, assume that a source with a SNR of 10 is observed at 150 MHz. The error in the differential phase will then be about 0.1 rad, leading to an error in differential TEC of 1.8 mTECU,

The TEC along a single line-of-sight may vary with the position at which the line-of-sight is passing through the ionosphere. These density variations can either be structured, for example Traveling Ionospheric Disturbances (TIDs) or density ducts [4], or unstructured. In the latter case, the ionospheric density variations can be described by a turbulence model. In both cases, the density variations can be characterized by a typical length scale. For example, Kolmogorov turbulence can be described by the phase structure function [3]

$$D(r) = \left(\frac{r}{r_{\text{diff}}} \right)^{\beta}, \qquad (2)$$

where $\beta = 5/3$ for Kolmogorov turbulence and the diffractive scale r_{diff} is the length scale on which the average phase variance between two points separated by r_{diff} is equal to 1 rad^2. The structure function description can also be applied to wave-like structures. For a pure sine wave, r_{diff} is a fraction of its wavelength, where the fraction is determined by the amplitude of the wave, and $\beta = 2$.

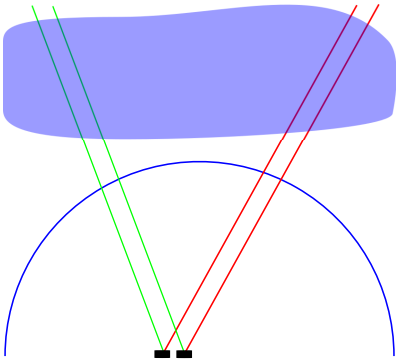

Figure 1. Ionospheric calibration of small arrays using a spherical phase screen to describe ionospheric effects. The red and green lines represent lines-of-sights towards two calibration sources and the blue semi-circle shows the hemisphere on which the phase screen function is defined.

Small arrays are arrays whose maximum baseline is smaller than the diffractive scale $r_{\rm diff}$. This definition implies that, for small arrays, the phase variance induced by the differential ionospheric TEC on the longest baseline in the array is less than 1 rad^2 for each source detected. However, the TEC observed towards different sources may differ significantly, in particular for arrays providing a large field-of-view. This scenario is sketched in Fig. 1. This small array scenario is applicable to, for example, an individual station of the Low Frequency Array (LOFAR, [5]), the Murchison Widefield Array (MWA, [6]), the core of the low-frequency element of the Square Kilometre Array (SKA-low, [7]) or the core of the LOFAR.

Calibration sources that are bright enough to be detected with a SNR of at least 5 when an individual receiving element is correlated against all other receiving elements, can be used to estimate an ionospheric phase contribution per receiving element. The lines-of-sight from all receiving elements to that calibrator intersect a facet of a sphere around the array as depicted in Fig. 1. For this facet, the phase solutions can be combined to get a continuous phase function over the facet. Each calibration source thus provides information about the phase function for a single facet on the sphere. If the calibrator density is high enough, the facets will overlap, which enables us to combine the phase solutions by exploiting the continuity of the electron density distribution in the ionosphere. The reconstructed spherical phase screen can then be used to make appropriate corrections in the imaging stage to make undistorted reconstructions of the weaker sources between the calibration sources.

The accuracy of the phase estimate for each puncture point (the intersect point of the corresponding line-of-sight with the sphere) depends on the SNR towards each calibration source, which is given by [8]

$$\mathrm{SNR} = \frac{S}{2k_{\rm B}}\frac{A_{\rm e}}{T_{\rm sys}}\sqrt{B\tau(N-1)}, \qquad (3)$$

where S is the flux of the calibration source, $k_{\rm B}$ is the Boltzmann constant, $A_{\rm e}/T_{\rm sys}$ is the sensitivity of an individual receiving element measured in units of m^2/ K, B is the integration bandwidth, τ is the integration time and N is the number of receiving elements in the array. The accuracy of the phase estimates is typically about $1/\mathrm{SNR}$.

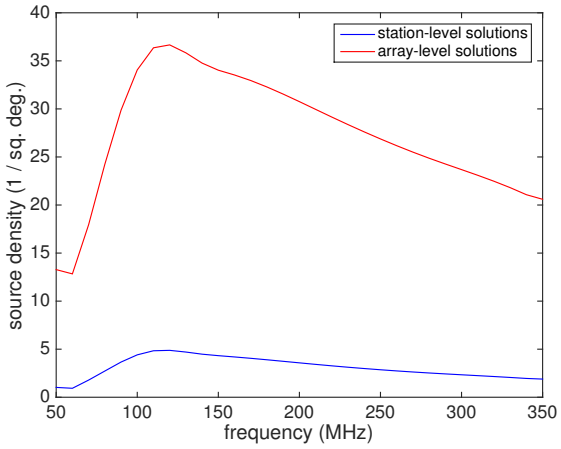

Figure 2. Density of calibration sources with SNR > 5 for the SKA core when solving for an ionospheric phase per station per source (station-level solutions) and when solving for source position shifts (array-level solutions).

If the array is sufficiently small, no significant phase differences may be measured towards each of the calibration sources and the spherical phase screen function will be constant. As only phase differences can be measured (and thus matter), no corrections are required to compensate for ionospheric distortions. The next level of complexity is a linear phase function across the array for each of the calibration sources. Such a linear gradient causes the apparent source positions to be shifted with respect to the nominal source positions. For a point source, this position shift can be measured in the image plane with an accuracy of about [9]

$$\Delta l = \frac{\theta_{\rm HPBW}}{2\mathrm{SNR}_{\rm array}}, \qquad (4)$$

where $\theta_{\rm HPBW}$ is the half power beam width of the point spread function of the array and $\mathrm{SNR}_{\rm array}$ is the SNR of the source as observed by the full array, which is given by

$$\mathrm{SNR}_{\rm array} = \frac{S}{2k_{\rm B}}\frac{A_{\rm e}}{T_{\rm sys}}N\sqrt{B\tau}. \qquad (5)$$

It is important to note that the SNR in the image plane is about a factor $\sqrt{N}$ higher than the SNR per station. As a result, much weaker sources can be used as calibrator for this method, which increases the density of calibration sources significantly. This approach is therefore particularly suitable for small arrays consisting of small receiving elements (with small effective area) such as MWA, where this method was introduced [10].

To illustrate the impact of the choice between the two methods presented above, Fig. 2 shows the typical density of calibration sources for the 225 stations in the SKA core area

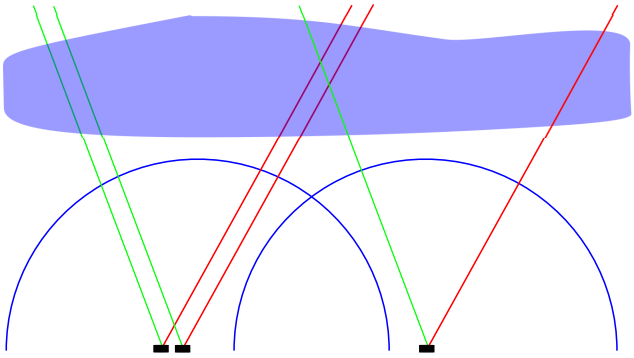

Figure 3. Ionospheric calibration of large arrays using spherical phase screens for subarrays or receiving elements with large separation. The red and green lines represent lines-of-sight towards two calibration sources and the blue semi-circles show the hemispheres on which the phase screen functions are defined.

[11] assuming that the SKA stations adhere to the SKA sensitivity requirement [12]. These curves assume that ionospheric calibration is performed with a frequency resolution of 1 MHz and a time resolution of 10 s.

3 Measurements with large arrays

In large arrays, the baselines may be significantly larger than the diffractive scale. The lines-of-sight towards each source may therefore pass through different turbulence cells. Also, there may be lines-of-sight that pass through almost the same point at the average height of the ionosphere, but point towards different calibration sources and therefore sample the ionosphere along a different path when the 3-D structure of the ionosphere is taken into account. This situation is sketched in Fig. 3.

A straightforward extension to the phase screen model described in the previous section is to define a phase screen per individual receiving element or per subarray of receiving elements with a size smaller than the diffractive scale. As the number of lines-of-sight available to construct each of these phase screens will be significantly smaller than for the small-array case presented earlier assuming the same number of stations, each phase screen needs to be constructed based on (far) fewer puncture points. To ensure enough puncture points, a sufficient number of calibration sources needs to be available within the field-of-view. Equation (3) then implies that either the sensitivity per receiving element (A_e/T_{sys}) needs to be above a given threshold value or the array needs to be large enough (sufficiently large N). This threshold can be determined using source statistics [13].

The approaches discussed so far can all be considered image domain descriptions of the effects of the ionosphere. A fundamentally different way to describe the ionospheric effects is by a phase function defined in a plane at some height above the aperture that describes the phase variations experienced over the aperture of the telescope. This route is taken in the Source Peeling and Atmospheric Modeling (SPAM) method [14]. As presented in [14], SPAM uses a single phase screen at an assumed average height of the ionosphere above the aperture. It is, however, straightforward to extend this method to multiple screens at different heights by linear superposition. To avoid an excessive increase in the number of model parameters required, that superposition can be collapsed into a single screen by integration towards a screen below the ionopshere that effectively integrates over all layers defined. This approach has been found to work well for arrays whose receiving elements have a relatively small field-of-view, such as the Very Large Array (VLA) and the Giant Metrewave Radio Telescope (GMRT) as, in those cases, the spread in angles at which the lines-of-sight intersect the ionosphere is limited, which allows the integration over multiple layers to work.

4 Array-level versus element-level modeling

If a single phase screen for the entire array is constructed by estimating the phases for individual lines-of-sight, the accuracy of the phase estimates to which the phase function is fitted, is limited by the SNR per receiving element given by Eq. (3). This may pose a significant constraint on the achievable image quality if the phase function is not sufficiently smooth, i.e., if the introduction of the phase function does not lead to a significant reduction in the number of degrees of freedom compared to the number of puncture points. This observation follows from the following argument.

The errors in the phase screen fit will be dominated by the phase errors of the weakest calibration sources. Let us suppose that the SNR on these puncture points is 5. When the corresponding sources are imaged, their SNR will be approximately $5\sqrt{N}$, which follows from comparing Eq. (5) with Eq. (3). Unfortunately, in our assumed scenario, in which the errors do not average out over the puncture points, the full phase error introduced by the single station adds noise to the image at a level that is $\sqrt{N}$ times the thermal noise. This effect can be mitigated by using the phase solutions obtained to subtract the calibration sources to the noise level. However, the same phase errors then affect the sources that are just not bright enough to be used as calibration sources, i.e, sources with a SNR of 3 for example. This will then increase the noise level in the image at the location of those sources by a factor $(3/5)\sqrt{N}$, which is still much larger than 1 for most arrays.

This issue does not arise when a phase screen is determined by using source position shifts as those are determined in the image plane thereby taking advantage of the full array sensitivity, neither does this issue arise when a phase screen is fitted per receiving element as in that case the errors on the direction dependent corrections made for the receiving elements average out during the imaging process at the same rate as the SNR improves. We therefore con-

clude that approaches using a single phase screen for the entire array should only be used if the reduction in degrees of freedom is sufficiently large to ensure at least a $\sqrt{N}$ reduction in the estimation errors on the individual puncture points.

5 Conclusions

In this paper, I gave an overview of currently used ionospheric calibration schemes in radio astronomy. For small arrays, whose maximum baseline is still smaller than the typical diffractive scale of the ionospheric structure function, the array can be calibrated by a global phase screen solution obtained either by fitting a phase function to the phase solutions obtained per receiving element and per calibration source or by constructing a phase function based on the observed position shifts. For large arrays, whose maximum baseline is (much) longer than the diffractive scale, ionospheric calibration is typically done using a phase screen per receiving element or a phase screen across the aperture. Global solutions have the disadvantage that the reduction in degrees of freedom should ensure at least a $\sqrt{N}$ reduction in the estimation errors of the individual puncture points.

The phase estimation errors for individual puncture points correspond to differential TEC measurements in the order of 1 mTECU. A radio interferometric array provides a high density of puncture points over the aperture of the array. An interesting side effect of ionospheric calibration in radio astronomy is therefore that radio astronomical arrays provide information about the ionosphere that is complementary to conventional ionospheric soundings, which typically measure the absolute TEC over much larger areas with typically an order of magnitude lower accuracy.

6 Acknowledgements

This work is supported by the Netherlands Organisation for Scientific Research. The author is co-chair of the resolution team on ionospheric calibration for the SKA and would like the members of the resolution team for sharing their insights. They are: Peter Dewdney, Natasha Hurley-Walker, Huib Intema, Chris Jordan, Maaijke Mevius, Daniel Mitchell, Maria Rioja and Cathryn Trott.

References

[1] C. M. Ho, A. J. Mannucci, U. J. Lindqwister, X. Pi, and B. T. Tsurutani,"Global ionospheric perturbations monitored by the Worldwide GPS Network," *Geophysical Research Letters*, **23**, 22, November 1996, pp. 3219-3222, doi: 10.1029/96GL02763.

[2] J. L. Garrison, S. G. Lee, J. S. Haase, and E. Calais, "A method for detecting ionospheric disturbances and estimating their propagation speed and direction using a large GPS network," *Radio Science*, **42**, 6, December 2007, doi: 10.1029/2007RS003657.

[3] M. Mevius et al., "Probing ionospheric structures using the LOFAR radio telescope," *Radio Science*, **51**, 7, July 2016, pp. 927–941, doi: 10.1002/2016RS006028.

[4] S. T. Loi et al., "Real-time imaging of density ducts between the plasmasphere and ionosphere," *Geophysical Research Letters*, **42**, 10, May 2015, pp. 3707–3714, doi: 10.1002/2015GL063699.

[5] M. P. van Haarlem et al., "LOFAR: The Low Frequency Array," *Astronomy & Astrophysics*, **556**, A2, August 2013, pp. 1–53, doi: 10.1051/0004-6361/201220873.

[6] S. J. Tingay et al., "The Murchison Widefield Array: The Square Kilometre Array Precursor at Low Radio Frequencies," *Publications of the Astronomical Society of Australia*, **30**, 7, January 2013, doi: 10.1017/pasa.2012.007P.

[7] P. E. Dewdney, P. J. Hall, R. T. Schilizzi, and T. J. L. W. Lazio, "The Square Kilometre Array," *Proceedings of the IEEE*, **97**, 8, August 2009, pp. 1482–1496, doi: 10.1109/JPROC.2009.2021005.

[8] S. J. Wijnholds, "Fundamental accuracy limits of ionospheric characterization by radio interferometers," *URSI Atlantic Radio Science Conference (AT-RASC)*, May 2015, doi: 10.1109/URSI-AT-RASC.2015.7303209.

[9] E. B. Fomalont, "Image Analysis." In: G. B. Taylor, C. L. Carilli, and R. A. Perley (eds.), "Synthesis Imaging in Radio Astronomy II," *ASP Conference Series*, **180**, 1999.

[10] D. A. Mitchell et al., "Real-Time Calibration of the Murchison Widefield Array," *IEEE Journal of Selected Topics in Signal Processing*, **2**, 5, October 2008, pp. 707–717, doi: 10.1109/JSTSP.2008.2005327.

[11] P. E. Dewdney and R. Braun, "SKA1-low configuration coordinates - conplete set," *Tech. report SKA-TEL-SKO-0000422*, SKA Office, Manchester (UK), 31 May 2016.

[12] W. Turner, "SKA phase 1 system requirements specification," *Tech. report SKA-TEL-SKO-0000008*, SKA Office, Manchester (UK), 6 December 2016.

[13] S. J. Wijnholds, J. D. Bregman, and A. van Ardenne, "Calibratability and its impact on configuration design for the LOFAR and SKA phased array radio telescopes," *Radio Science*, **46**, RS0F07, November 2011, pp. 1–10, doi: 10.1029/2011RS004733.

[14] H. T. Intema et al., "Ionospheric calibration of low frequency radio interferometric observations using the peeling scheme - I. Method description and first results," *Astronomy & Astrophysics*, **501**, 3, July 2009, pp. 1185–1205, doi: 10.1051/0004-6361/200811094.